The Astrophysical Journal, 834:86 (17pp), 2017 January 1 doi:10.3847/1538-4357/834/1/86
© 2017. The American Astronomical Society. All rights reserved.

CHALLENGING SOME CONTEMPORARY VIEWS OF CORONAL MASS EJECTIONS. II. THE CASE FOR ABSENT FILAMENTS

T. A. Howard[1], C. E. DeForest[1], U. G. Schneck[2], and C. R. Alden[3]
[1] Southwest Research Institute, 1050 Walnut Street, Suite 300, Boulder, CO 80302, USA; howard@boulder.swri.edu
[2] Department of Earth, Planetary, and Space Sciences, University of California, Los Angeles, CA 90095, USA
[3] Department of Atmospheric Sciences, Lyndon State College, 1001 College Road, Lyndonville, VT 05851, USA
Received 2016 September 7; revised 2016 November 3; accepted 2016 November 4; published 2017 January 4

ABSTRACT

When a coronal mass ejection (CME) appears in a coronagraph it often exhibits three parts. This "classic" three-part configuration consists of a bright leading edge, a dark circular- or teardrop-shaped cavity, and a bright core within the cavity. It is generally accepted that these are manifestations of coronal plasma pileup, the driving magnetic flux rope, and the associated eruptive filament, respectively. The latter has become accepted by the community since coronagraph CMEs have been commonly associated with eruptive filaments for over 40 years. In this second part of our series challenging views on CMEs, we present the case that the inner core of the three-part coronagraph CME may not be, and in the most common cases is not, a filament. We present our case in the form of four exhibits showing that most of the CMEs in a broad survey are not associated with an eruptive filament at the Sun, and that the cores of those CMEs that are filament-associated do not geometrically resemble or consist of material from the associated filament. We conclude with a discussion on the possible causes of the bright CME core and what happens to the filament material postlaunch. We discuss how the CME core could arise spontaneously from the eruption of a flux rope from the Sun, or could be the result of a mathematical caustic produced by the geometric projection of a twisted flux rope.

Key words: solar–terrestrial relations – Sun: corona – Sun: coronal mass ejections (CMEs) – Sun: filaments, prominences

Supporting material: animation

1. INTRODUCTION

Solar filaments play an important role in the development of coronal mass ejections (CMEs). This is not only because they convey information about the configuration of the photospheric magnetic field but because many models describing the launch of CMEs involve filaments (e.g., Martin et al. 1985; Sturrock 1989; van Ballegooijen & Martens 1989; Fong et al. 2002; Zhang & Low 2004). The observational connection between filaments and CMEs has been established since the discovery of the coronagraph CME (Tousey 1973) and perhaps even prior to that (e.g., Athay & Moreton 1961). Early results show that CMEs have been more closely associated with filaments on the solar surface than, say, the flare (e.g., Gosling et al. 1976; Joselyn & McIntosh 1981). The disappearance of an on-disk solar filament, or its corresponding off-limb eruptive prominence, are regarded as standard near-Sun signatures of the eruption of a CME (e.g., Burlaga et al. 1982; Bothmer & Schwenn 1994, and references therein). It is important to recognize such signatures, because the departure of the CME itself is rarely observed in solar disk imagery.

Filaments (also called prominences when observed above the solar limb) are believed to be a main component of CMEs when they are observed by coronagraphs. The so-called "classic" CME (Illing & Hundhausen 1985) consists of three parts; a bright leading edge followed by a dark cavity within which lies a bright core. It is generally accepted (e.g., Bothmer & Schwenn 1998; Forbes 2000) that these are physical manifestations of coronal plasma pileup, the driving magnetic flux rope, and the erupting filament/prominence, respectively. The inner core is often the brightest component of this three-part configuration. Figure 1 shows a popular image of a classic three-part CME from the LASCO-C3 coronagraph on board *SOHO*. Note the size and brightness of the core component compared with the rest of the CME. Howard (2015c) found that this particular bright core contributed 40% to the total intensity of the CME in this image. This three-part configuration is very commonly observed; early papers state that more than 70% of large coronagraph CMEs contain the bright core component (e.g., Munro et al. 1979; Webb & Hundhausen 1987).

Despite their common association with CMEs, filaments are rarely observed at large distances from the Sun. Researchers searching for filament signatures with in situ spacecraft have sought large abundances of low-temperature ions (e.g., Schwenn et al. 1980; Cane et al. 1986; Skoug et al. 1999; Lepri & Zurbuchen 2010) and in some cases solar wind regions of high densities accompanying low temperatures (e.g., Yao et al. 2010; Sharma & Srivastava 2012). While there is some debate as to whether these signatures are what we might expect for filaments at large distances from the Sun, only a small ratio of these signatures have been found in the proximity of CMEs that are measured in situ. For example, Lepri & Zurbuchen (2010), after a systematic survey of 283 in situ CMEs, found that only 4% of them contained such a signature, while a recent study by Wood et al. (2016) sought filaments accompanying CMEs in white-light heliospheric images at angles larger than 20° from the Sun, and found only two throughout the nine-year history of the *STEREO* mission. While the core component is smaller than its CME counterpart, and one can reasonably expect that a large portion of them will miss an in situ spacecraft that has been struck by the larger CME, the relative sizes between the core and CME (the core component in Figure 1 is around 1/3 the pixel width of the overall CME) would likely suggest that there would be a larger impact ratio

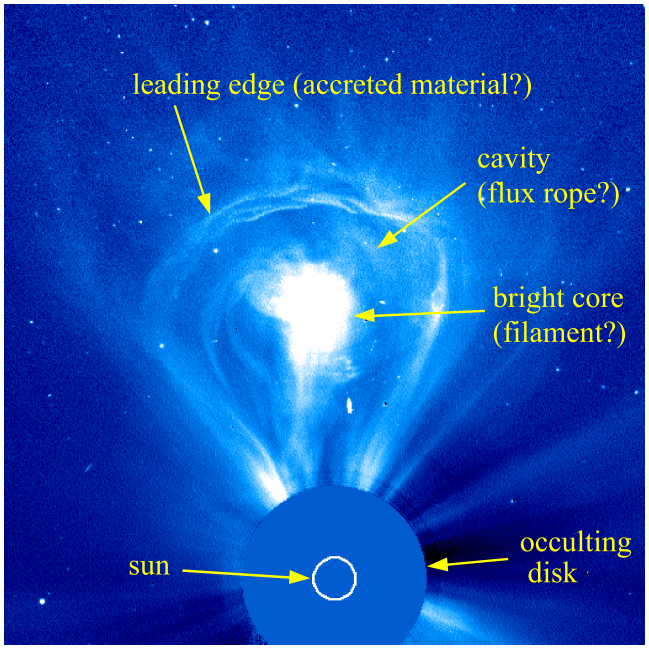

Figure 1. Popular image of a CME from the LASCO-C3 coronagraph on *SOHO*, obtained on 2000 February 27 at 07:42UT. This depicts the "classic" three-part configuration that is commonly observed in larger CMEs. The bright core component is generally believed to be the filament that originated on the solar surface. In this image, the core contributed 40% to the total intensity of the CME (Howard 2015c).

than the 4% found by Lepri & Zurbuchen (2010). Furthermore, the relative brightnesses of the core components in the coronagraph images imply that a significant portion should be detectable by heliospheric imagers farther from the Sun. There appears to be a disconnect between our current understanding of the CME-filament relationship and the observational evidence which, perhaps, requires a change of perspective.

1.1. Recent Work on Filaments at Large Distances from the Sun

While the physics describing filament emission was heavily studied in the 1960s and 1970s (e.g., Athay 1968, 1970; Illing et al. 1975; Landman & Illing 1976; Poland & Munro 1976; Schmahl & Hildner 1977; Landman et al. 1978) and extensive work continues to date on noneruptive and pre-eruptive filaments (see the book by Vial & Engvold 2015, for a recent review), little work has been done on eruptive filaments after they have departed the Sun. A few papers have emerged that present theoretical treatments for the neutral-ionic content of filaments in the corona (e.g., Athay et al. 1987; Rudawy & Heinzel 1992; Vranjes et al. 2004), but observational studies have practically ceased since the mid-1980s. Between the time of the *Solar Maximum Mission (SMM)* studies by Athay and Illing (Illing & Hundhausen 1985; Athay & Illing 1986; Illing & Athay 1986; Athay et al. 1987) and 2015, we are aware of only a single paper that has presented measurements of an eruptive filament at distances beyond a few solar radii ($R_\odot$). This study by Mierla et al. (2011) confirmed the low-polarization signature that is characteristic of Hα emission (Breit 1925; Hyder 1965; Poland & Munro 1976) for a single CME-associated eruptive filament observed by the COR1 coronagraph on *STEREO-B*.

Since 2015 three papers have appeared that explore the properties of eruptive filaments beyond distances of 5 $R_\odot$. Howard (2015a) presented measurements of a single filament using polarization measurements with COR1-B. Extending the work of Mierla et al. (2011), he found that the polarization of the filament increases with increasing distance from the Sun, reaching the "Thomson-scattering domain" by the time it had reached a distance of 7 ± 2 $R_\odot$. This was interpreted as a measurement of the ionization rate of neutral hydrogen in the filament and compared favorably with theoretically determined predictions of this rate. Using these results, Howard (2015b) went on to measure the mass and kinematic evolution of the same filament. A third publication in 2016 by Wood et al. presented 3D reconstructions of geometric and kinematic properties of two filaments and their associated CMEs, one of which was the same as that studied by Howard. They found that filaments are not necessarily tied to the magnetic properties of their accompanying CME and that the geometry of the filaments remained intact out to many tens of $R_\odot$. The two filaments studied by Howard (2015a, 2015b) and Wood et al. (2016) were clear cases of CME cores that were actual filaments that originated at the Sun and propagated through the heliosphere. Although additional such filaments were sought by Wood et al. (2016) they found only those two in the *STEREO*/HI-2 data sets for the entire duration of the *STEREO* mission.

It should be clear from these studies that filaments that are recognized far from the Sun are very rare, very bright, and very energetic. It is also noteworthy that one of the two *STEREO*-era filaments, the one on 2011 June 7, has attracted attention by many researchers, not for the quantity of material that escaped the Sun, but for the large quantity that was seen to drain back into the Sun postlaunch. Papers exploring this aspect of launch for that filament include Innes et al. (2012), Gilbert et al. (2013), Carlyle et al. (2014), and Thompson & Young (2016).

This paper is the second part of a series of papers challenging contemporary views of CMEs. The first part, by Howard & Pizzo (2016), presents the case that some CMEs are blast waves originating from an impulsive energy release at the Sun, a finding that has implications for the present paper (Section 6). In the present paper, we address the question as to why so few eruptive filaments are observed far from the Sun. The two filaments that have been studied may be the only two that have escaped the solar corona in the nine years of the *STEREO* mission. We present the case that many of the filaments that appear in coronagraph images of CMEs are not filaments at all, but rather a natural consequence of flux rope launch or an optical illusion brought about by the geometrical overlay of a twisted, 3D-extended magnetic flux rope.

2. OUR STUDY

Observations of eruptive filaments were obtained from the Atmospheric Imaging Assembly (AIA) on board the *Solar Dynamics Observatory* (*SDO*, Lemen et al. 2012), EUVI on board *STEREO* (Howard et al. 2008), and on the ground by the GONG network (http://gong.nso.edu/). CME observations were obtained from LASCO on *SOHO* (Brueckner et al. 1995), and the COR1 and COR2 coronagraphs on board *STEREO* (Howard et al. 2008). The *STEREO* spacecraft occupy an orbit around the Sun such that they have increased in angular separation from the Sun–Earth vector since their launch in late 2006. *STEREO-B* ceased transmitting in 2014 October and at the time of writing, it had not been reactivated. Meanwhile,

STEREO-A has recommenced transmission since it passed behind the Sun for much of 2015, and continues to operate nominally.

We selected 42 CMEs spanning two years from 2010 December until 2012 December. We sought CMEs that clearly exhibited the classic three-part configuration in the LASCO coronagraphs and were not complicated by multiple eruptions or other features that obscured their geometry. Our decision to begin the selection in 2010 December was to avoid the risk of a possible solar filament erupting in a blind spot on the solar globe. In 2011 February the *STEREO* spacecraft were oriented such that their EUVI fields of view covered the entire solar globe (see the NASA press release at www.nasa.gov/mission_pages/stereo/news/entire-Sun.html). We decided that by 2010 December, the gap between the *STEREO-A* and *STEREO-B* fields of view was sufficiently small that some part of an erupting filament would be observable even if it originated from within the gap.

Our event selection was assisted by the CDAW LASCO catalog (Yashiro et al. 2004). This was used as a quicklook reference to assist in the identification of the presence of a CME and bright core, but we performed all of our measurements and analysis. Table 1 provides a list of our selected 42 CMEs.

Note that we deliberately excluded two CMEs that have already been confirmed as containing eruptive filaments. These have been explored in detail by many workers and are described by Wood et al. (2016) as being the only two filaments that they could confirm as being within CMEs for the entire *STEREO* mission to date. They can, therefore, be regarded as two examples of three-part CMEs that do contain an eruptive filament at their core, and we describe them in more detail in Section 4.

3. RESULTS

In adherence to the courtroom analogy, we present our results as a series of four "exhibits," each offering plausible evidence that coronagraph CMEs do not involve escaping filaments. Our first two exhibits eliminate the majority of our selected CMEs as candidates for containing an eruptive filament, while the last two focus on the remaining CMEs, specifically attacking the commonly held belief that observed CME cores are erupting filaments.

3.1. Exhibit A: Many CMEs Do Not Have an Associated Eruptive Filament

Figure 2 contains a combination of images showing a CME that erupted on 2011 November 02 (#11 in Table 1). The CDAW catalog lists the onset time and location of this CME as 20:05UT and at a central position angle of 54°. This CME exhibited a gradual acceleration throughout its passage through the LASCO field of view, making it difficult to identify its exact onset time. An arcade near the northeastern limb relative to *SDO* was observed to brighten at around 22:00UT (Figure 2(b)), with a soft X-ray emission peak classed at M4.3. The CME and its bright core were already in the LASCO-C2 field of view at this time (see Figure 2(a)). This appears to be reminiscent of a post-eruptive arcade of the kind described by Tripathi et al. (2004), and we interpret it as a signature of the disconnection of at least part of the CME flux rope via magnetic reconnection low in the corona. In that sense, the arcade is an indicator of the location of that part of the CME flux rope after it has departed from the Sun. Figure 2(c) shows the view relative to *STEREO-B*; we see that it was at around 30° west of the Sun-*STEREO-B* vector (the location of the *STEREO* spacecraft relative to the Earth is shown in Figure 2(b)). Much later, at around 03:20UT on 2011 November 03, an eruptive filament was observed near the site of the post-eruptive arcade (not shown). This later filament, most easily seen in the 304 Å camera on AIA, erupted when the CME and its bright core were well beyond a distance of 10 $R_\odot$ from the Sun.

Following close inspection of every wavelength of AIA and EUVI-B, we found no evidence of an eruptive filament at any time throughout 2011 November 02. Likewise, we found no disappearing filaments or eruptive prominences in the ground-based Hα images throughout the day. We found nothing, in fact, that could be interpreted as the departure of what could become the bright core of the CME in the LASCO images indicated in Figure 2(a). In other words, we found no eruptive filament to be associated with the three-part CME on 2011 November 02. Likewise, we found no eruptive filament associated with 15 of the CMEs in Table 1; we have denoted these as "Category-A" CMEs. This means that 36% of our three-part CMEs were not associated with any observable eruptive filament. Figure 3 shows LASCO/C2 images of a further four such CMEs. In panel (d) we overlay an outline of what appears to be a geometrical configuration that was common for the cores of many CMEs. The implications of this are discussed in Section 5.1.2.

3.2. Exhibit B: Other CMEs Do Not Have an Eruptive Filament at the Correct Time and/or Location

Those CMEs in Table 1 for which an eruptive filament was associated, either spatially or temporally, but not both, were designated as "Category-B" CMEs. Figure 4(a) exhibits a combination of AIA and LASCO images showing the CME that erupted on 2012 January 27 (#15 in Table 1). A filament eruption was observed in the proximity of this CME, which is shown in Figure 5(c) relative to *SDO*. This filament erupted at around 03:30UT, but did not appear to move far from the Sun.

The near-Sun signatures of the formation and departure of this CME were investigated at length by Sun et al. (2015). They identified it as a signature of the tether cutting of a CME flux rope from the Sun (see, e.g., Sturrock 1989). We agree with their assessment, and provide images from the 171 Å imager on AIA in Figure 5. In this figure, we indicate the location of the CME core in LASCO with a blue arrow. The following three properties should be apparent:

1. The cavity seen in AIA is the same as the cavity in LASCO-C2.
2. No eruptive filament passes anywhere near the AIA cavity, yet a bright core is clearly seen within the LASCO-C2 cavity.
3. The eruptive filament seen to the north of the tether cutting is spatially separated from the core of the CME in LASCO-C2.

We conclude from this that the eruptive filament is not the same feature as the bright core that is seen within the LASCO-C2 image of the CME cavity. Since some readers may not be willing to conclusively rule out the presence of

Table 1
List of Selected CMEs for Our Study

#	Date and UT Time	Category	COR1 CME (Filament)	Hα Filament	Figure
1	2010 Dec 02 11:12	A	AB (n)	none	…
2	2010 Dec 12 02:48	A	B (n)	none	…
3	2010 Dec 14 15:36	C	AB (AB)	15:10	7(a), 11, 8(a)
4	2010 Dec 30 09:36	C	A (n)	05:45	…
5	2011 Jan 13 18:12	A	A (n)	none	…
6	2011 Jan 14 19:00	A	n (n)	none	…
7	2011 Mar 11 20:12	A	A (n)	data gap	…
8	2011 Apr 10 00:24	B-T	AB (n)	none	11
9	2011 May 01 14:24	A	AB (n)	none	3(a)
10	2011 Oct 25 06:24	C	A (n)	05:40	10
11	2011 Nov 02 20:00	A	n (n)	none	2, 11
12	2011 Nov 20 14:48	C	A (A)	14:55	11
13	2011 Dec 10 07:24	B-T	B (n)	none	…
14	2012 Jan 08 02:12	B-DT	AB (n)	none	…
15	2012 Jan 27 03:47	B-D	AB (n)	none	4, 5, 11
16	2012 Jan 31 16:48	C	A (n)	13:50	6(a)
17	2012 Feb 06 00:00	B-T	AB (n)	none	11
18	2012 Feb 25 10:24	A	n (n)	none	…
19	2012 Feb 29 14:24	A	B (n)	none	…
20	2012 Mar 06 08:12	A	AB (n)	none	…
21	2012 Mar 24 09:12	A	B (n)	none	3(b)
22	2012 Apr 02 02:12	B-T	AB (n)	data gap	…
23	2012 Apr 14 19:00	C	A (n)	data gap	6(b), 11
24	2012 Apr 27 19:00	A	B (B)	none	3(c), 11
25	2012 Apr 29 09:36	B-DT	B (B)	none	…
26	2012 May 02 07:12	B-T	A (n)	none	…
27	2012 Jun 03 12:24	A	AB (n)	none	…
28	2012 Jun 08 03:12	B-T	AB (AB)	none	11
29	2012 Jun 08 17:57	C	AB (n)	14:50	11
30	2012 Jun 18 15:00	B-T	B (B)	data gap	11
31	2012 Jun 27 10:48	C	AB (A)	10:40	7(b), 11
32	2012 Jul 13 00:36	B-T	AB (AB)	none	11
33	2012 Jul 27 00:06	C	AB (AB)	(07/26) 22:30	7(c), 11
34	2012 Aug 10 00:45	B-DT	AB (n)	(08/09) 21:30	11
35	2012 Aug 20 13:16	A	AB (A)	none	3(d), 11
36	2012 Sep 23 14:12	C	AB (n)	14:40	…
37	2012 Oct 08 08:36	B-T	AB (n)	08:20	11
38	2012 Oct 22 00:48	C	AB (B)	00:15	8(b)
39	2012 Oct 26 09:48	B-T	AB (n)	06:00	11
40	2012 Nov 10 14:12	A	B (n)	none	…
41	2012 Nov 14 12:48	C	A (A)	12:10	11
42	2012 Nov 18 20:36	C	AB (AB)	19:40	6(c), 8(c), 11

Note. Each of these was selected, because they were clear three-part CMEs that occurred during the time where there was full coverage of the sun. Dates and times match those listed in the CDAW catalog for easy reference and the category of each CME (A = no associated eruptive filament; B = associated filament that did not match in time (T) and/or location (D) with the CME core; C = associated eruptive filament could potentially be the CME core) is listed. The fourth column indicates whether the CME was observed with one of the COR1 coronagraphs on *STEREO-A* (A) and/or *STEREO-B* (B), and an indication of whether the CME core was observed in COR1 is given in brackets (n = no core was observed in either COR1). The fifth column indicates whether an associated filament was observed in the ground Hα imagery, and the time of its eruption or the last image obtained prior to its disappearance is given where appropriate. Finally, the figure of this paper in which the CME appears is listed in the final column.

an eruptive filament, given that one occurred somewhere near the CME, we placed CMEs of this kind into a different category to those we described in Section 3.1; they are "Category-B" CMEs. CMEs in this category were further divided into "B-T," where the erupting filament was roughly in the correct location, but did not erupt at the time needed for it to have reasonably become the core within the CME observed by LASCO, and "B-D," where the timing matched, but the location did not. The CME shown in Figures 4 and 5 was categorized as B-D, since it did not show a good match in location, yet its timing suggested that it could not be completely ruled out as being associated with the CME.

Table 1 shows that there were 14 Category-B CMEs. In each case we ruled out direct launching of the associated filament as the cause of the CME core, on the basis of spatial or temporal mismatch in the launched filament with the core. This means that without any further evidence we may already regard 69% of our three-part CMEs as not containing a filament that erupted off the Sun.

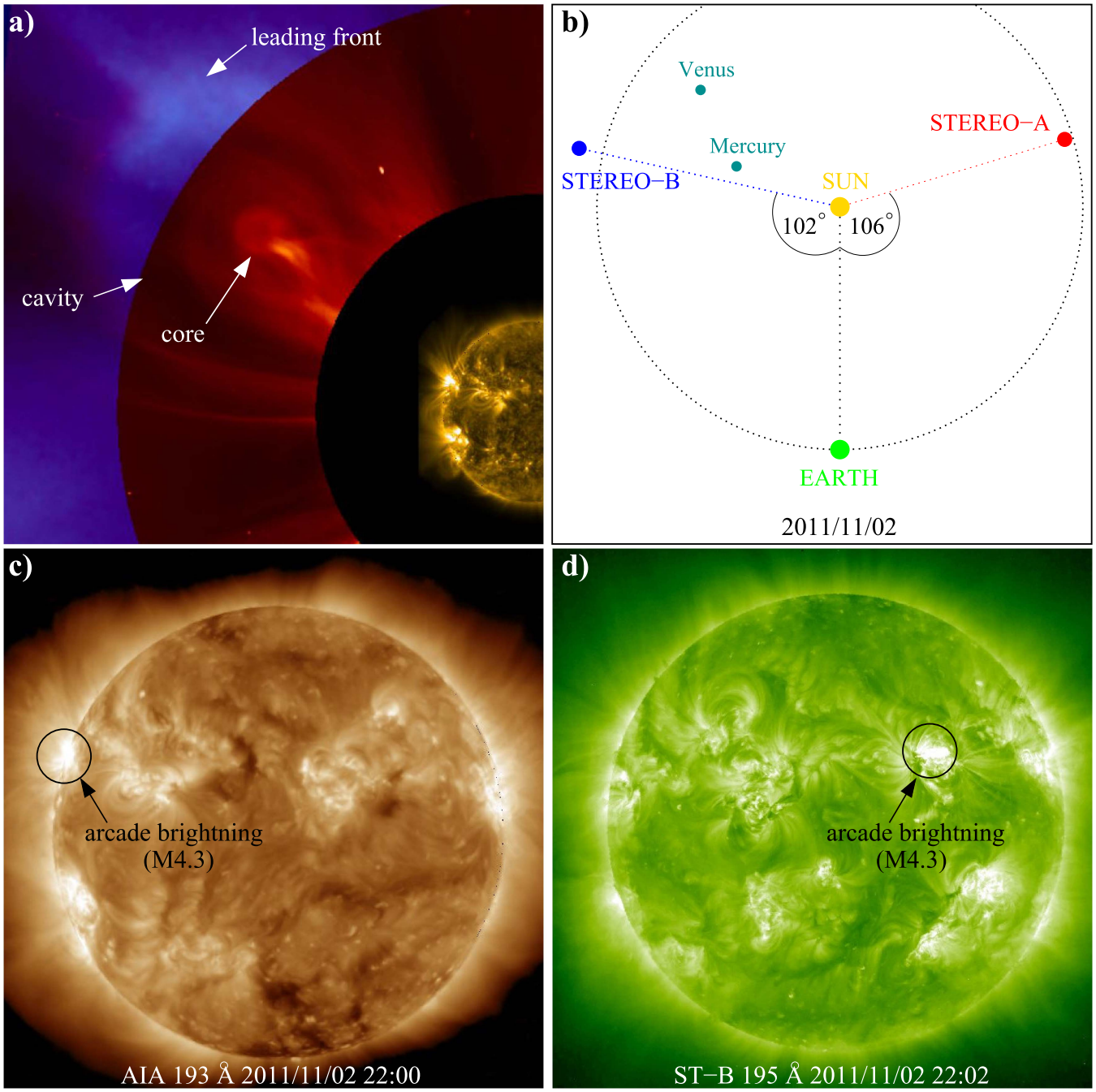

Figure 2. (a) An example of a Category-A CME that erupted from the Sun on 2011 November 02 (#11 in Table 1). Shown is a combination of images from the C2 (red) and C3 (blue) coronagraphs on LASCO, and the 171 Å imager (gold) on AIA. The times for each image are 23:06UT, 23:12UT and 23:09UT, respectively. The CME clearly exhibits the classic three-part configuration in LASCO (labeled). (b) The configuration of the *STEREO* spacecraft relative to the Earth at the time of this CME. At this time, *STEREO-B* was 102° east of the Sun–Earth vector. (c) AIA 193 Å image, taken at 22:00:10UT of an arcade brightening (circled) associated with the disconnection of the CME. (d) EUVI 195 Å images, taken at 22:02UT, from *STEREO-B*. The same arcade brightening from panel (c) is circled. While this CME was associated with a post-eruptive arcade, no associated eruptive filament was observed in any wavelength from *SDO* or EUVI.

3.3. Exhibit C: Eruptive Filaments Do Not Have the Same Geometrical Appearance as the Observed CME Core

This section (exhibit) is primarily based on the assumption of a ballistic filament. A ballistic filament would not change its geometry until the bulk of its material has become ionized. We know that Hα emission persists within filaments at a few solar radii from the Sun (Athay & Illing 1986; Illing & Athay 1986; Mierla et al. 2011; Howard 2015a), and the geometric reconstructions of two filaments by Wood et al. (2016) showed that they expanded self-similarly out to many tens of solar radii (see their Figure 11). This, to us, is sufficient evidence upon which to assume that the geometry of the filament will not change very much, at least for the purposes of one of our four "exhibits."

Table 1 shows that 13 of our CMEs are classed as "Category-C." These are CMEs which were associated with an eruptive filament that occurred at a time and location such that an observer could reasonably deduce that they may have become the bright core within the three-part CME observed by the coronagraphs.

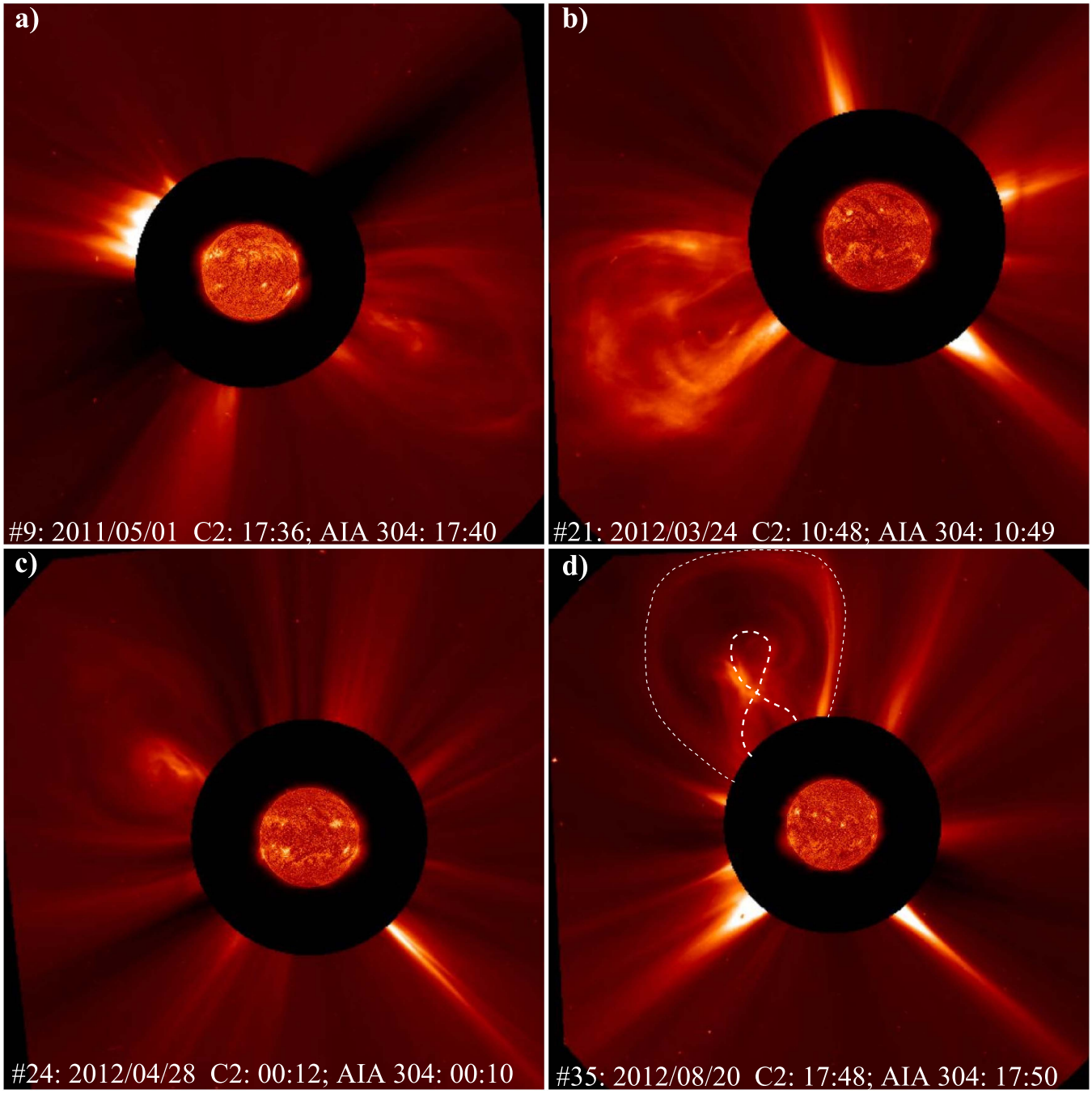

Figure 3. Four more Category-A CMEs (additional to that in Figure 2), which are CMEs that were not associated with an eruptive filament at the Sun. Dates and times for the LASCO-C2 images are: (a) 2011 May 01 17:36UT (#9); (b) 2012 March 24 10:48UT (#21); (c) 2012 April 28 00:12UT (#24); (d) 2012 August 20 17:48UT (#35). The corresponding image from the AIA 304 Å imager has been included in each image. An overlay of the geometrical structure of the leading edge and inner core of the CME has been included (dashed) in panel (d). Note the "figure-8" geometry of the inner core.

These were in a clear minority on our list (31%), and in the following section we present evidence that even in these cases the bright CME core is not the same physical feature as its associated eruptive filament at the Sun. Note that the CME we present in Figure 1 also falls into the Category-C classification.

Figure 6 shows three of the Category-C CMEs, #16 (2012 January 31), #23 (2012 April 17), and #42 (2012 November 18). The solar disk is shown from three different wavelengths and a LASCO-C2 image is also shown. The filament in the AIA 304 Å image and the core of the CME are expanded and placed alongside each other for comparison. It should be clear in these cases that the geometry of the filament does not resemble that of the core of the CME in C2. We found this to be the case for 10 of our 13 Category-C CMEs. For the remaining three of our events the appearance of the filament did have a similar appearance to the CME core in LASCO-C2. These were #3 (2010 December 14), #31 (2012 June 27), and #33 (2012 July 27) and are shown in Figure 7.

It should be noted that there are physical reasons why a filament may change its geometrical appearance as it erupts

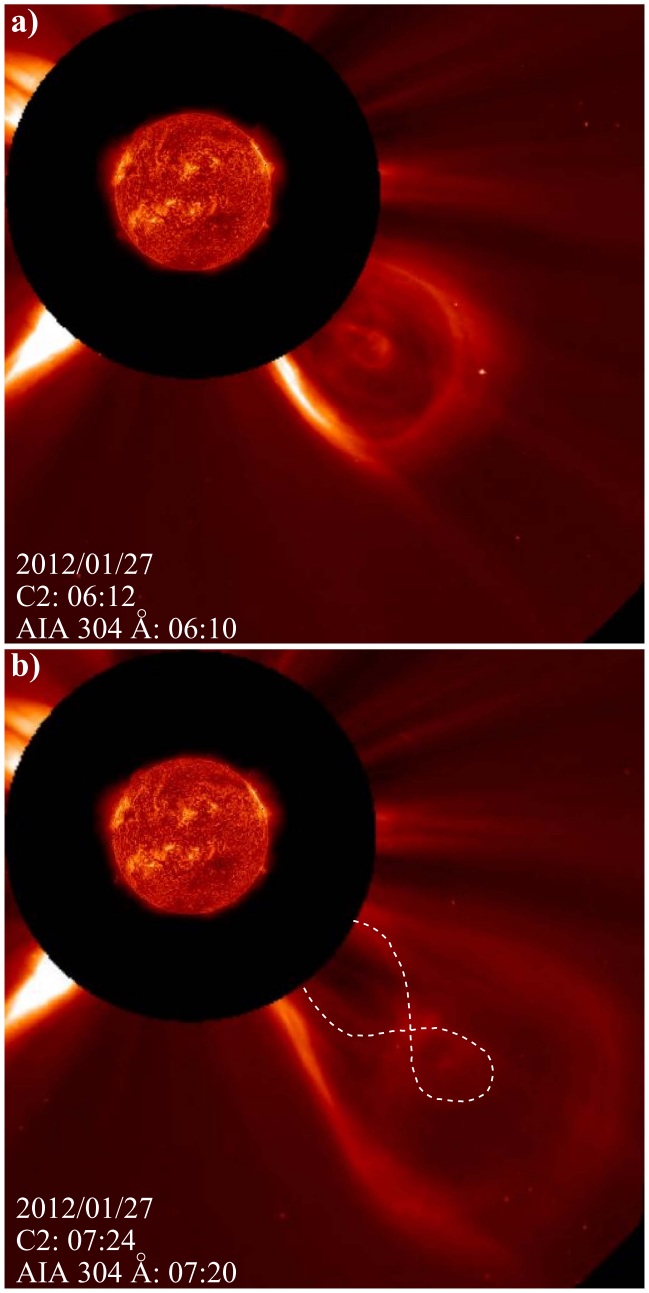

Figure 4. Images from LASCO-C2 and the 304 Å imager on AIA of a CME that erupted on 2012 January 27 (#15 in Table 1). Shown are the three-part CMEs in C2 an hour apart, at (a) 06:10UT and (b) 07:20UT. Again, we see the figure-8 geometry of the CME core in panel b (overlayed with a dashed curve).

through the solar corona and that the 304 Å wavelength is outside the passband of LASCO. Hence, this exhibit alone is certainly not sufficient to demonstrate that they are not the same feature. We explore some of these physical possibilities in Section 5.

3.4. Exhibit D: Hα Emission Is Not as Expected for Filaments

If the bright cores observed in the coronagraphs are the same as the filaments we periodically see erupting from the Sun, we would expect them to be bright in Hα, since prominences are bright in Hα images when they depart the

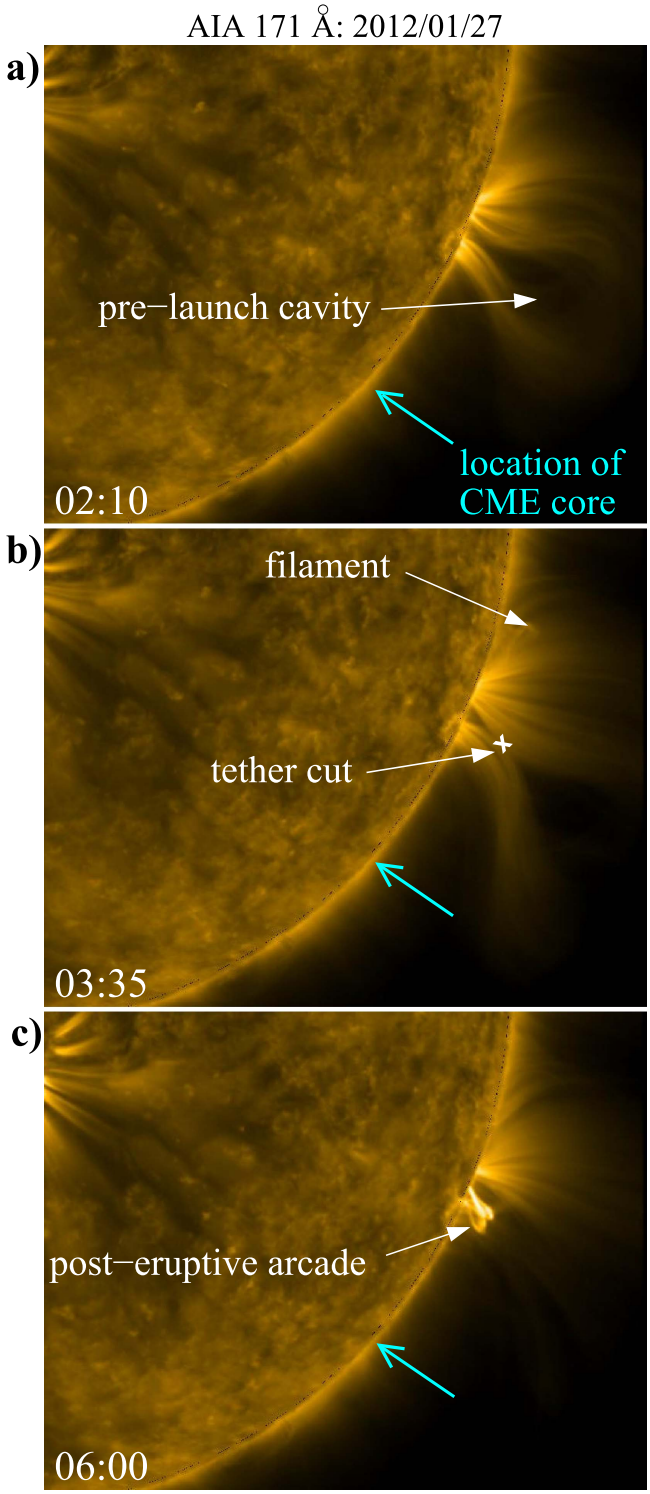

Figure 5. Images from the 171 Å imager on AIA during the launch of the CME on 2012 January 27. Shown are three images from before, during, and after the launch. (a) Prelaunch image at 02:10UT showing the cavity that becomes the cavity in the C2 image. (b) Image at 03:35UT showing a merger of the structure behind the cavity as it launches. This is cited by Sun et al. (2015) as evidence of the tether-cutting launch mechanism. (c) postlaunch image at 06:00UT showing the post-eruptive arcade that has often been associated with postlaunch CMEs (e.g., Tripathi et al. 2004). In all three panels the location of the core of the associated LASCO CME in Figure 4, projected to the solar disk, is indicated with the blue arrow, and is some considerable distance from the location of the filament, but note that projection is effective in the LASCO-C2 image.

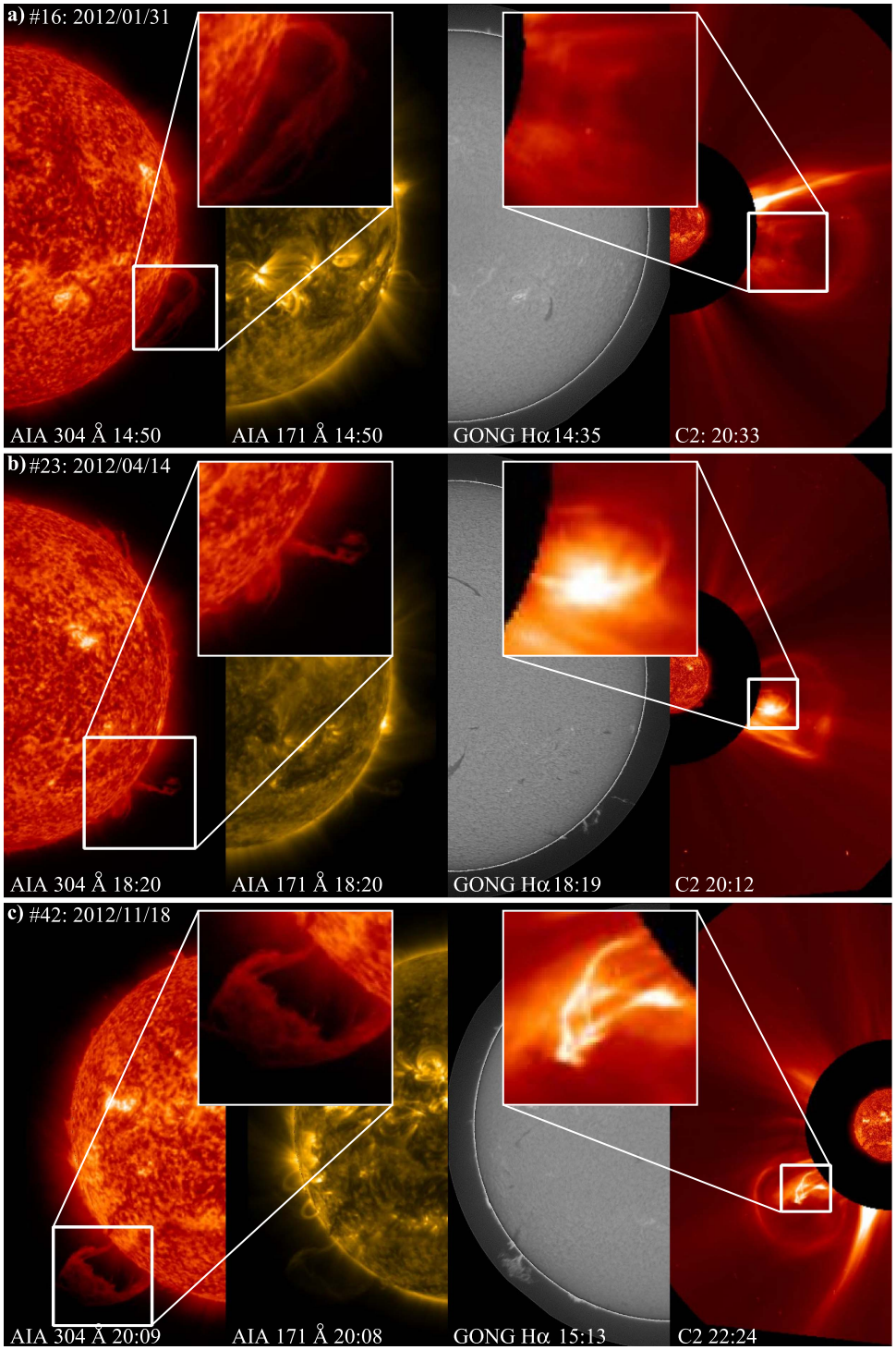

Figure 6. Three examples of Category-C CMEs that exhibited an inner bright core that did not geometrically resemble their accompanying filament. From Table 1 the three CMEs are (a) #16 (2012 January 31), (b) #23 (2012 April 14), and (c) #42 (2012 November 18). In each case, solar disk images from AIA 304 and 171 Å and the GONG Hα filament are shown, along with the LASCO-C2 image of the CME and its bright core. The 304 Å filament and C2 CME core are expanded and placed alongside each other for direct comparison. In each case, the geometry of the filament does not resemble the core of the CME.

Sun (e.g., Figure 6). None of the currently operating spacecraft coronagraphs possess the ability to isolate Hα emission,[4] but they do have the capability to observe polarized light and have a passband that contains the Hα line. As we briefly mentioned in Section 1.1, researchers have shown that Hα emission exhibits a consistently low polarization. This is brought about by the Hanle effect and a possible collisional depolarization (Breit 1925; Hyder 1965; Poland & Munro 1976; Heinzel et al. 1996). We can contrast this with

[4] LASCO does have Hα filters, but they have not been used in C2 since 1998 and have never been used in C3.

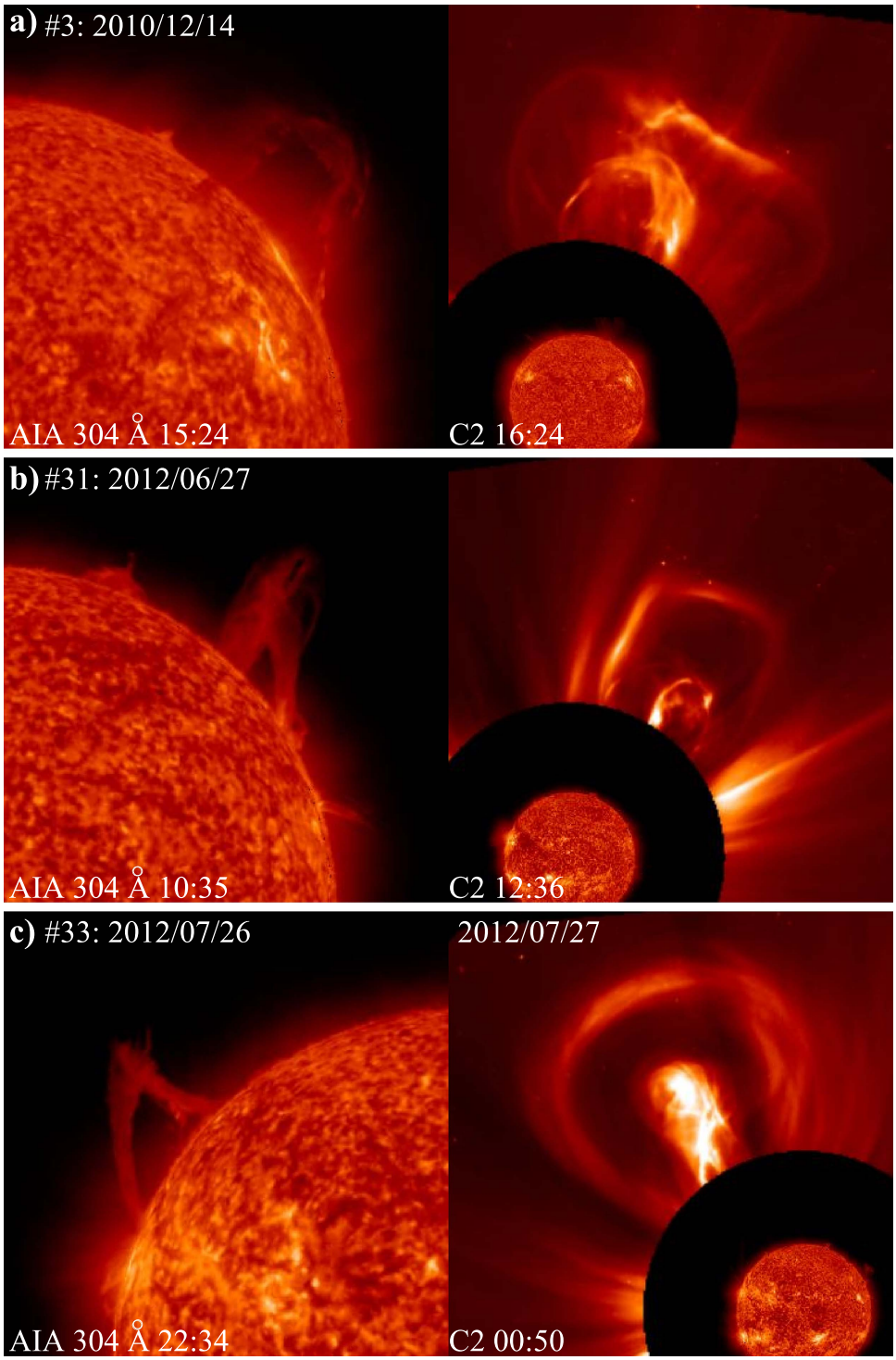

Figure 7. Images of the three Category-C CMEs containing a bright core that does resemble the geometry of their associated filament. The three events are (a) #3 (2010 December 14), (b) #31 (2012 June 27), and (c) #33 (2012 July 26). In each case, we show an image of the filament from AIA 304 Å and the LASCO-C2 image, aligned for ease of comparison.

the Thomson-scattering contribution that is typically the dominant signal observed by coronagraphs after background subtraction, as Thomson-scattered light has a comparatively strong polarization that is dependent on the scattering geometry (e.g., Minnaert 1930). Such a contrast has been performed on CME-associated filaments observed by the COR1 coronagraph on *STEREO-B* by Mierla et al. (2011) and Howard (2015a). In both of those studies the presence of a nearly unpolarized core within the CME was found despite the CME being close to the plane of the sky relative to *STEREO-B*, where its Thomson-scattered characteristics would exhibit a high polarization. In both papers, this was cited as evidence for the presence of a filament that was bright in Hα.

The COR1 coronagraph on *STEREO* is well suited to detect Hα emission, as its relatively narrow passband is centered on the unshifted Hα emission wavelength of 6563 Å. It also routinely provides polarization triplets that enable the production of polarized (pB) images with a relatively high cadence of ~5 minutes. *STEREO*/COR2 is less well suited for this purpose for two reasons; first, because it has a passband where the inner edge of the FWHM lies near the Hα line (so that Hα will only be around half as bright relative to the surrounding Thomson-scattered signal), and later in the *STEREO* mission it provided polarized image triplets with decreasing cadence. LASCO provides polarization triplets only once per day, and as such were not useful for our study (see Howard 2015a, for more details).

Clearly, an eruptive filament will need to pass through the COR1 field of view before moving farther into the corona observed by COR2 and LASCO. Given the characteristics of the COR1 detector and assuming that an eruptive filament is still bright in Hα while it is within 4 $R_\odot$ of the Sun, we can reasonably expect the following observations if the CME core is an eruptive filament:

1. The CME core is very bright in COR1;
2. The CME core exhibits a low polarization in COR1.

Howard (2015a) and Mierla et al. (2011) showed the presence of both of these signatures for two CMEs that were confirmed to contain an eruptive filament (see Figure 3 of Howard 2015a and Figures 1 and 2 of Mierla et al. 2011). One of these is discussed further in Section 4 and the other is outside the time range imposed by our selection criteria.

Of the 42 CMEs listed in Table 1, 13 (31%) were associated with a CME core that we could identify in COR1 for *STEREO-A* and/or *STEREO-B*. As we can see from Table 1, most of them (7/13) were identified as Category-C, or CMEs that had an associated filament that could have become the coronagraph CME core. Four were classed as Category-B, while only two were Category-A.

We produced polarized COR1 images for each of the 13 CMEs for which a CME core was visible in COR1. Following the methodology of Howard (2015a), these were calibrated using the processing pipeline of Thompson et al. (2010). This pipeline combines each polarization triplet into an image calibrated into units of excess polarized radiance, or pB. We used these to produce pB/B images, where B is the total (unpolarized) radiance.

Figure 8 shows images from COR1 for three of the Category-C CMEs (#3, #38, and #42 in Table 1). Following Figure 3 of Howard (2015a), these are shown in total (B) and polarized (pB/B) formats. A filament that is bright in Hα would appear in these images as being very bright in the B images and very dark (pB/B ~ 0.2 (Howard 2015a)) in the pB/B images, while the surrounding CME could be bright or dark depending on its location relative to the plane of the sky (e.g., Howard & DeForest 2012). We can see that in each case the core of the CME, while bright and structured in the B image, does not appear as a dark feature in the pB/B image; in panel (a) it is a bright feature, in panel (b) it is invisible, and in panel (c) there is a slightly less bright feature that is nowhere near as dark as expected for Hα emission. This means that none of them appear to exhibit Hα emission despite their proximity to the Sun. We found this to be the case for each of the 13 CMEs for which a core was found in COR1.

Finally, we searched the ground-based Hα images for evidence of an erupting filament for each CME; our findings are shown in the 5th column of Table 1. An Hα filament (prominence) was seen departing the Sun in 15 cases, all of which corresponded to the filament observed with *SDO*/AIA. No Hα filaments were found for any of the Category-A CMEs, while 10 were Category-Cs, meaning that the vast majority (77%) of our Category-C CMEs were associated with an Hα filament. We were able to investigate the polarimetry properties of seven of the Category-Cs, but we cite the absence of a bright core in the COR1 images as evidence for their absence there, since we would expect an Hα filament to be bright in an instrument as sensitive to Hα emission as COR1. Note that the filament reported by Howard (2015a) was so bright that it saturated COR1-B for 45 minutes.

4. DO ANY FILAMENTS SURVIVE FAR FROM THE SUN?

There were over 2800 CMEs with a large variety of sizes and structures that were listed in the CDAW catalog during the time period of our event selection. If we regard those that have an apparent angular width relative to LASCO $\geqslant 90^\circ$ as "large" CMEs, then the catalog lists around 450 that could be regarded as large. Of those, only two have so far been confirmed to contain eruptive filaments that have been tracked to large distances from the Sun. These were associated with CMEs that departed the Sun on 2011 June 07 and 2012 August 31 and the large-distance evolution of both have been investigated by Howard (2015a, 2015b) and Wood et al. (2016). A summary of these works is provided in Section 1.1.

While we found no peer-reviewed articles on the 2012 August 31 CME other than those of Howard and Wood et al., several papers have been published on the 2011 June 07 CME that focus on the eruption of its associated filament. Innes et al. (2012) describe how filament material reaching heights of 4 $R_\odot$ spread out across a 600″ area on the solar limb (relative to *SDO*) as it fell back into the solar atmosphere, and that the filament began to break up almost immediately after launch. Carlyle et al. (2014) found that the column density of hydrogen within the in-falling filament material was comparable to that of a typical prelaunch filament, Thompson & Young (2016) traced the trajectory of many of the filament fragments as they returned to the Sun, while Gilbert et al. (2013) investigated the interaction of the falling filament material with the solar atmosphere.

The important features of these two filaments that are pertinent to our study are that they were unusually large and bright and that, for one of them at least, the filament fragmented soon after its launch and a large proportion of its material fell back into the Sun. Furthermore, following a survey of the entire heliospheric imager data set from the *STEREO* mission, these were the only two filaments that Wood et al. (2016) found at distances beyond 15 $R_\odot$ from the Sun.

5. DISCUSSION

Our evidence suggests that none of our selected 42 CMEs contained an eruptive filament that originated at the Sun. This is despite the facts that all of them were classic three-part

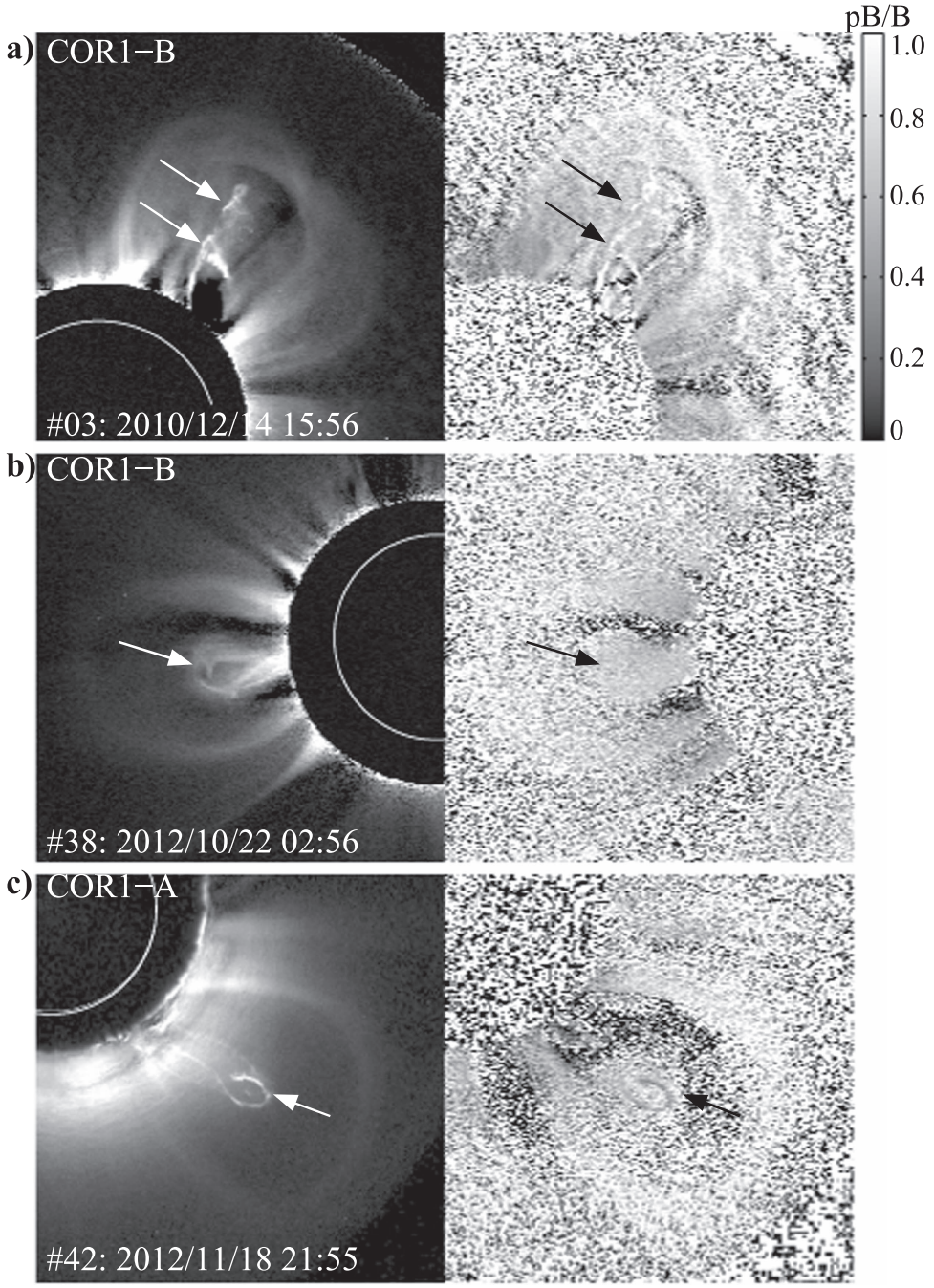

Figure 8. Total and polarized brightness images of three selected CMEs. The selected CMEs are (a) #3 (2010 December 14), (b) #38 (2012 October 22), and (c) #42 (2012 November 18). The left column shows "total" brightness (B) images produced following the removal of the constant bright background. The right column shows "polarized" brightness as a ratio with total (pB/B). This format follows that of Figure 3 in Howard (2015a). If the CME core were dominated by Hα emission, we would expect it to be bright (white) in the B image, but very dark (black) in the pB/B image. We see that in all three cases the CME core either also appears bright as in panel (a) or does not appear as a sufficiently dark feature as in panels (b) and (c). We cite this as evidence that the CME cores are not dominated by Hα emission. These CMEs were selected, because they had the brightest and most structured appearance in the B images, but we found the same for all of the 13 CMEs in Table 1 for which a core was found in COR1.

CMEs and that we were able to observe the entire solar disk at multiple wavelengths for each one. Simple inspection of the images (Sections 3.1 and 3.2) was sufficient evidence to suggest that a large majority (69%) did not contain an eruptive filament, while further analysis revealed the same to be true of the remaining 31%. We believe that this is likely to be true for the vast majority of three-part CMEs, and, as suggested by Wood et al. (2016), may even be true for every CME observed during the *STEREO* mission, apart from the two described in Section 4.

In light of our evidence, we are obliged to ask two questions:

1. If the bright core of a coronagraph CME is not a filament, then what is it?
2. What happens to the filament material between its departure from the Sun and the arrival of its associated CME in coronagraph images?

At this point, we offer speculation as to the answers to these questions. Addressing the second question first, a clue may lie in the nature of the eruption of one of the filaments that did make it to the coronagraph images. In Sections 1.1 and 4, we describe that much (possibly most) of the material making up the filament eruption associated with the 2011 June 9 CME drained back into the Sun. Filament draining has been observed in other CMEs (e.g., Howard & DeForest 2014), and the so-called "failed" filament eruption is said by Gilbert et al. (2013) to be the most commonly observed type (see also Gilbert et al. 2007). Filament draining has also been implemented into some CME evolution models (e.g., Chen 1996). If most of the filament material does drain back to the Sun, then there may not be enough material left over to be observable by coronagraphs for all but the most massive filaments.

Another possibility lies in the ionization of the filament as it evolves. While it begins its eruption being dominated by neutral particles, the *SMM* observations by Athay & Illing (1986) and later measurements by Howard (2015a) showed that filaments ionize as they move away from the Sun. Filaments comprised of neutral particles would retain their structures upon launch, but ionized filaments would assume the structures of their surrounding magnetic fields. If they were within a magnetic flux rope at the time of their ionization, their material would spread out across their respective field lines creating concentric rings that make up the flux rope cross-section (e.g., Low 1993; Bothmer & Schwenn 1998). When this happens, the filament material would become indistinguishable from the material making up the surrounding CME. We note that one might expect such behavior to be observable in at least some CMEs, since the total ionization of the filament would not occur until the CME was well within a coronagraph field of view. We found no evidence for such behavior and it was not the case for the two filaments discussed in Section 4 (Wood et al. 2016, their Figure 11), but we note that the existing imaging instruments are not well suited for a conclusive search.

A final possibility lies in the breakup of the filament structure as it ionizes. No geometrical breakup was noted in the observations of the filaments far from the Sun by Howard (2015b) and Wood et al. (2016), but the former did note a rapid dropoff of photometrically-inferred filament mass with increasing distance from the Sun and at least one of them lost most of its mass immediately after launch. This dropoff in filament mass (not density) at large distances was attributed to a possible dispersion of its material by Howard (2015b).

5.1. What Is the Bright Core?

Turning to the second question, we speculate as to possible causes for the bright cores observed within coronagraph CMEs and note that these may not necessarily be mutually exclusive. First, the bright loop-shaped core could be a cross-section of the CME flux rope. This could be caused by filament material ionizing and distributing its material around inner loops within the flux rope CME, or it could be a smaller end of the flux rope that appears as a small circular bright loop on projection. It has been shown observationally (e.g., Howard & DeForest 2014) that CMEs can expand at different rates and that different cross-sections of the same CME flux rope could appear as separate loops within a coronagraph image.

As the reader may realize, the definition of "filament material" becomes murky at this juncture. The elemental and ionic properties of noneruptive and pre-eruptive filaments are not well understood (Gilbert et al. 2002; Kilper et al. 2009, and references therein), and we do not have the capability to measure the ionic abundance of eruptive filaments beyond the fields of view of solar disk imagers. We can, therefore, only speculate at this stage as to the nature of the material comprising the filament at distances beyond around 5 $R_\odot$, except to say that the majority of the hydrogen atoms become ionized by the time the filament reaches this distance.

As neutrals give way to ions, however, the distinction becomes more difficult to identify. This is because by this time the filament and CME are made up of the same material (mostly hydrogen ions). We speculate in the prior section that the new filament ions could be distributed along the circular field lines comprising the CME flux rope. If this were to happen, then while the original filament mass would still be present within the CME, it would be physically and observationally indistinguishable from the rest of the CME. Of course, this is only one scenario that describes the possible

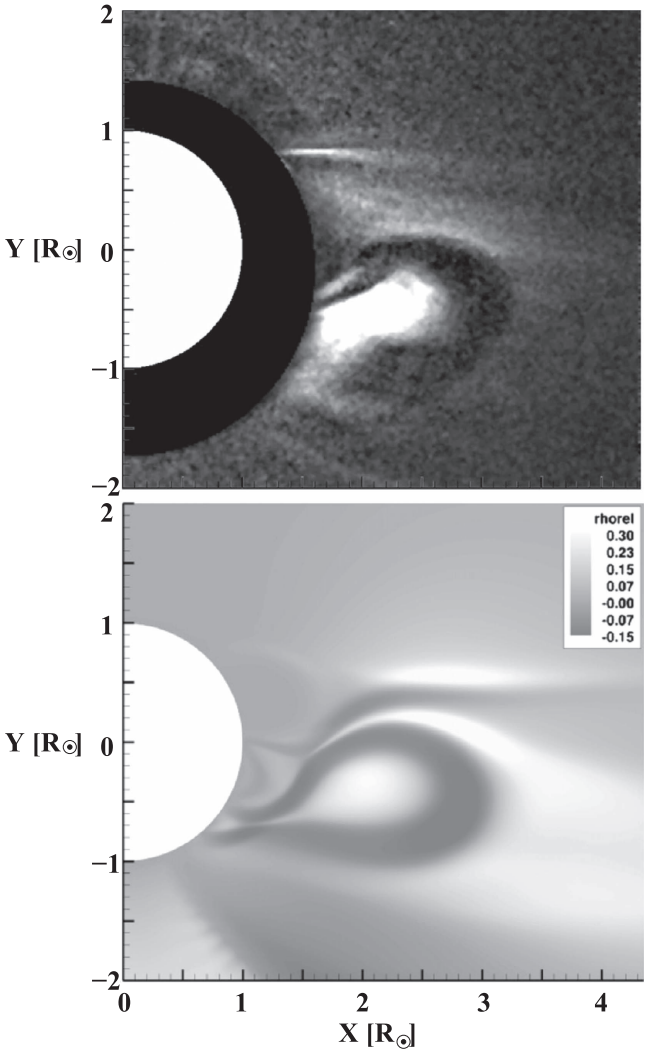

Figure 9. Reproduction of Figure 13 of Zuccarello et al. (2012), showing a comparison between a COR1-B image of a CME from 2009 September 21 (top) and the density distribution arising from a simulation of a CME. The model reproduces well the bright core feature within the CME, but this was a consequence of the evolution of the erupting CME flux rope and not from filament material. © AAS. Reproduced with permission.

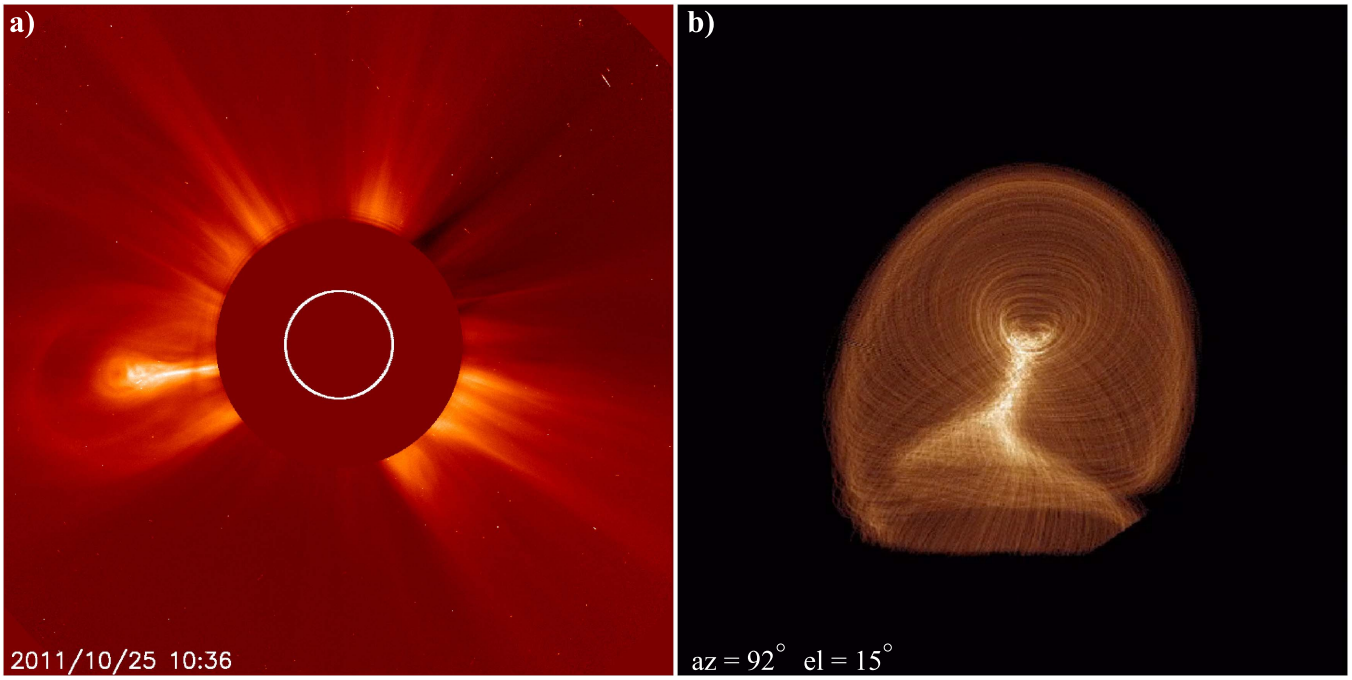

Figure 10. Side-by-side comparison of the LASCO-C2 coronagraph image of the CME on 2010 October 25 (#10 in Table 1) with a projection of our 3D model. This particular projection was taken at an angle of 92° relative to the starting location (see the online animated Figure 13). We see how the three-part configuration is reproduced well in the projected 3D model, including a close resemblance to the bright inner core. This demonstrates that no filament is needed to produce the appearance of the CME core.

fate of the original filament mass, and one that does not agree with the observations of the two filaments that have been verified to depart the Sun (Section 4). In the following subsections, we explore two possibilities for alternative sources for the bright CME core that do not require the presence of a filament.

5.1.1. Spontaneous Flux Rope Launch

Because CMEs are large-scale, energetic, and transient openings of a significant amount of previously closed magnetic flux, the plasma properties and flows associated with this large-scale magnetic field reconfiguration must play an important role in the resulting density distributions of and within the erupting magnetic structures. Models have shown that under such circumstances the density within the CME flux rope can increase, and under various physical conditions may give rise to internal density structures that resemble the bright cores within coronagraph CMEs. Simulations using the catastrophe model (Linker et al. 2001; Lin et al. 2004; Reeves et al. 2010) have shown that there is an increase in density within the flux rope that is formed ahead of the current sheet, and while the density drops off rapidly (three orders of magnitude) across a few solar radii, this model could possibly scale out to the distances observed by spacecraft coronagraphs. Models involving the breakout mechanism (Lynch et al. 2004; Zuccarello et al. 2012) have also shown a density enhancement with an evolving CME flux rope that look similar to CMEs as they appear in coronagraphs. Figure 9 shows one such comparison by Zuccarello et al. (2012). Here, the results of a simulation involving injected helicity compare favorably with a COR1-B image of a CME from 2009 September 21. The bright core within the CME is clearly shown here, but it does not arise from filament material in the simulation.

These models demonstrate that density enhancements within erupting CME flux ropes can occur spontaneously as a result of the eruption, and under certain conditions can reproduce well the bright core of the three-part CME configuration. None of this requires the presence of filament material.

5.1.2. A Geometric Solution

Modeling has shown that CMEs can be launched via the so-called kink (torus) instability (e.g., Fan & Gibson 2003, 2004; Török & Kliem 2003, 2005; Rachmeler et al. 2009), and Figures 3 and 4 show that the cores of many coronagraph CMEs exhibit a "figure-8" outline that is reminiscent of an extended 3D structure twisting on itself, and similar in geometry to the writhed flux ropes associated with pre-event active regions (Canfield et al. 1999).

To investigate how an expanding kinked and/or writhed magnetic structure may appear in a coronagraph image, we created a 3D geometric model of the magnetic structure within a hypothetical, simple, CME. In this geometrical reconstruction, we regard the CME as a large bundle of magnetic field lines twisted into a helical configuration and bent to form a loop that comprises the leading edge of the CME. The mathematical construction of this geometrical model is described in the Appendix.

Our geometric method emulates a bright shell of finite width, structured by the magnetic field. All variations of brightness in the online animated Figure 13 are due to so-called "caustic" or "line-of-sight" effects, within the geometric construction that emulates a simple writhed, twisted flux rope.

Figure 10 shows a C2 image of the CME on 2010 October 25 (#10 in Table 1) alongside a projection of our 3D geometric model. We see how the entire three-part CME is reproduced in this projection, including a close resemblance to the bright core within. A similar comparison for 20 of the CMEs in Table 1 is

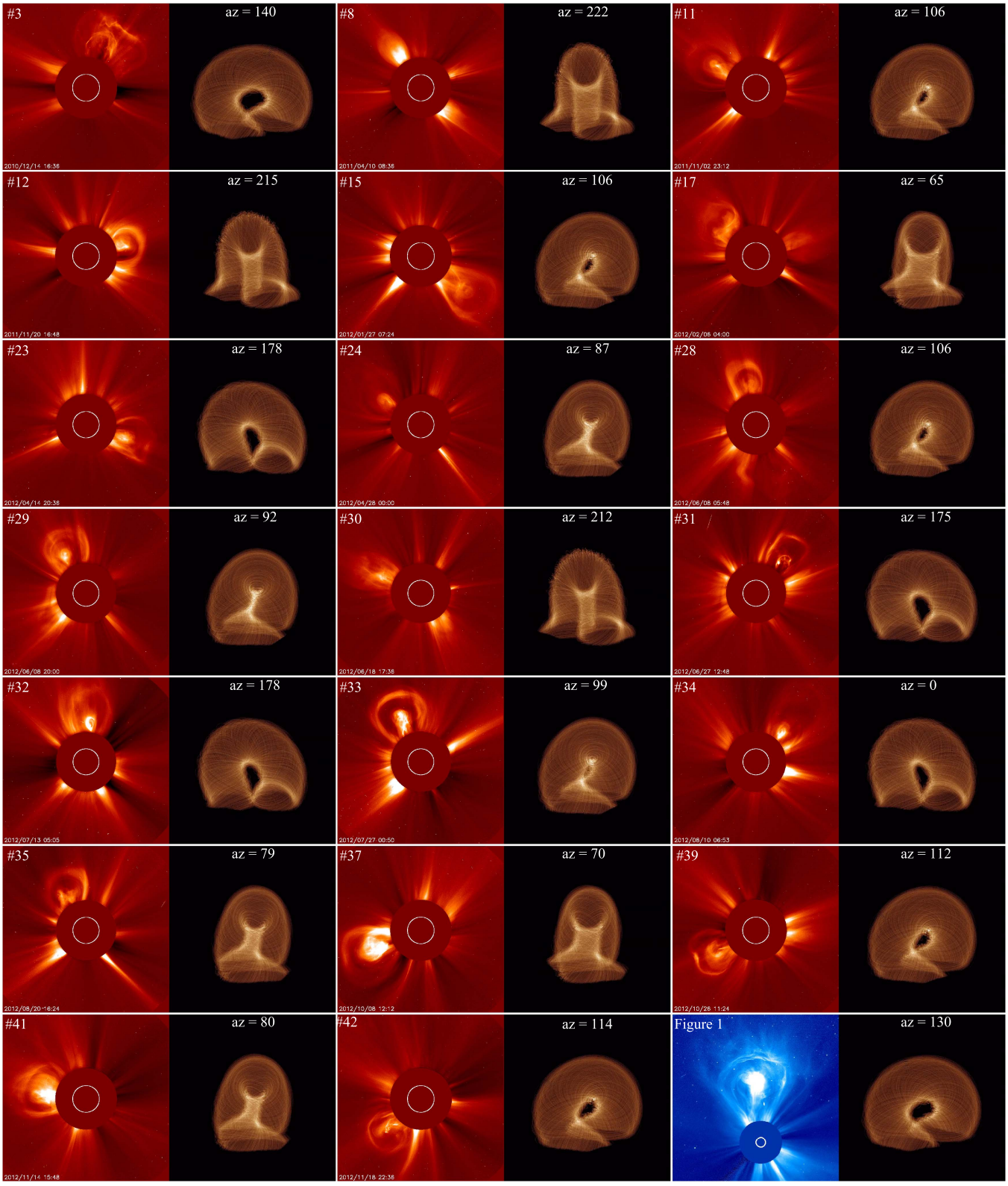

Figure 11. Coronagraph CME image comparisons with selected projections of our 3D geometric model for an additional 20 CMEs from Table 1. Only one parameter was allowed to vary: the azimuthal rotation of the model, which in all cases was viewed from 15° above the *xy* plane. This demonstrates that a good reconstruction of the appearance of each coronagraph CME can be achieved with the selection of an appropriate projection of even our simple geometric model. The details of each image, including the projection angle for reference to the online animated Figure 13, are provided in each case.

shown in Figure 11. As should be clear, we were able to reconstruct the appearance of each of the CMEs fairly well with even this simple geometrical model rotating along only a single axis.

This analysis shows that the suite of CMEs that we observed can all have their bright cores explained entirely via geometric projection. Projection effects, together with the complex shape of a generic writhed, twisted flux rope, are sufficient to produce

the observed menagerie of core shapes, even with only a single free parameter and a fairly generic loop shape.

6. SUMMARY AND CONCLUSIONS

We have presented evidence to support the claim that the bright core component of the classic three-part CME may not be a filament, but rather a consequence of the natural evolution of a launching flux rope or an optical illusion brought about by the geometry imposed by an extended twisted 3D flux rope erupting through the corona. This challenges a claim about CMEs that has been held since they were first detected by spacecraft coronagraphs. We present four "exhibits" with observational evidence to support this claim, including that the large majority of our selected three-part CMEs did not have an associated eruptive filament, that the geometry of associated eruptive filaments did not resemble the bright CME core in any way, and that the CME cores did not exhibit Hα emission in the COR1 field of view. These four exhibits show, together, that while filaments may be present in a small percentage of coronagraph CMEs, they are exceptional rather than a key aspect of the generic case. Furthermore, we found a stark contrast between the cores of our selected 42 CMEs and two cases that have been confirmed to contain eruptive filaments when the CMEs were within the fields of view of the coronagraphs. While the existence of those two confirmed filaments demonstrates that some coronagraph CMEs actually contain filaments, our evidence suggests that such cases are so rare that they are statistically insignificant. We provide modeling results that show how an eruptive filament is not needed to produce a bright CME core, and demonstrate how simple geometric projection into a 2D plane could provide the appearance of a bright core, with no special physics, only simple projected geometry coupled to the generic shape of a writhed flux rope.

CMEs are optically thin at visible wavelengths and the physics of Thomson scattering imposes a wide brightness distribution along their lines of sight (Howard 2015c, and references therein). This means that extended 3D features are projected into the 2D plane in their entirety. While simple analysis tends to regard CMEs as being narrow or confined within a single plane, our results stress the need to consider the 3D geometry of CMEs when reproducing their structures for scientific or forecasting purposes. While it is important to stress that CMEs are not symmetric in either geometry or kinematic evolution, we found that, even in the case of a simple bundle of geometric curves representing a kinked magnetic flux rope, we were able to reproduce well the three-part configuration of many coronagraph CMEs, including their bright core. It seems likely that, by varying the other parameters of this highly simple geometric model—including writhe rate, twist rate, vertical stretch factor, and vertical viewing angle—we could reproduce the appearance of many, or possibly all, CMEs as seen by coronagraphs.

We conclude with a comment on the implications for blast wave CMEs, the case which we presented in the first paper of our series (Howard & Pizzo 2016). It was suggested in that paper that a blast wave CME could possibly be identified by the absence of a filament in the coronagraph images. The inverse could also be true; in Section 2.2 (p. 3) of that paper it states that "the filament when observed by a coronagraph may provide an important signature for a CME flux rope." If the narrative in the present paper is correct, then the presence of a bright core within a coronagraph CME image may demonstrate the presence of a flux rope and, therefore, a high level of magnetic structure within the CME.

We thank NASA and NRL for their provision, calibration, and maintenance of the *SOHO* and *STEREO* data sets. We also thank NASA and Lockheed Martin for the *SDO*/AIA data set. We acknowledge the National Solar Observatory (which is operated by AURA, Inc., under a cooperative agreement with the National Science Foundation) for their maintenance of the GONG network and provision of data. For this work, TAH and CED were partially funded by the NSF SHINE Competition (grant AGS-1260321) and the AFOSR program (grant FA9550-14-0296), while the contributions of UGS and CRA were funded by the NSF REU Program (grant NSF-1157020).

APPENDIX
THE MATHEMATICAL CONSTRUCTION OF OUR SIMPLE GEOMETRIC CME MODEL

To provide a possible explanation for the appearance of the bright coronagraph CME core (Section 5.1.2), we modeled this system with the simplest possible geometric model: a collection of bright fibrils where each is described as a compound additive helix, reminiscent of Ptolemaic epicycles. We begin with an analytic semicircular loop (e.g., Anzer & Tandberg-Hanssen 1970), describing the unwrithed central loop of a CME flux rope, defined in the xz plane by:

$$\boldsymbol{r}_{\rm loop}(t) \equiv \begin{pmatrix} \cos(t) \\ 0 \\ \sin(t) \end{pmatrix},$$

where t is just a parametric variable ranging from 0 to π. We also define

$$\boldsymbol{M}_{\rm loop}(t) \equiv \begin{pmatrix} \cos(t) & 0 & \sin(t) \\ 0 & 1 & 0 \\ -\sin(t) & 0 & \cos(t) \end{pmatrix}$$

so that $\boldsymbol{M}_{\rm loop}\hat{x}$ points along the direction of the primary loop. We introduce a writhe offset:

$$\boldsymbol{r}_w(t) = r_w \boldsymbol{M}_{\rm loop} \begin{pmatrix} 0 \\ \cos(t\omega_w + \phi_w) \\ \sin(t\omega_w + \phi_w) \end{pmatrix}$$

for a writhe radius r_w, a rate ω_w, and a phase ϕ_w relative to the loop of ϕ_w. By setting those parameters, we define a writhed centerline for the field line bundle, which describes a simple circular helix:

$$\boldsymbol{r}_{\rm center}(t) \equiv \boldsymbol{r}_{\rm loop}(t) + \boldsymbol{r}_w(t).$$

Repeating the construction in the obvious way, we define

$$\boldsymbol{M}_w(t) \equiv \begin{pmatrix} 1 & 0 & 0 \\ 0 & \cos(t\omega_w + \phi_w) & \sin(t\omega_w + \phi_w) \\ 0 & -sin(t\omega_w + \phi_w) & cos(t\omega_w + \phi_w) \end{pmatrix},$$

so that M_w points along the direction of the writhe. Next, we calculated the offset of a single twisted flux line around the

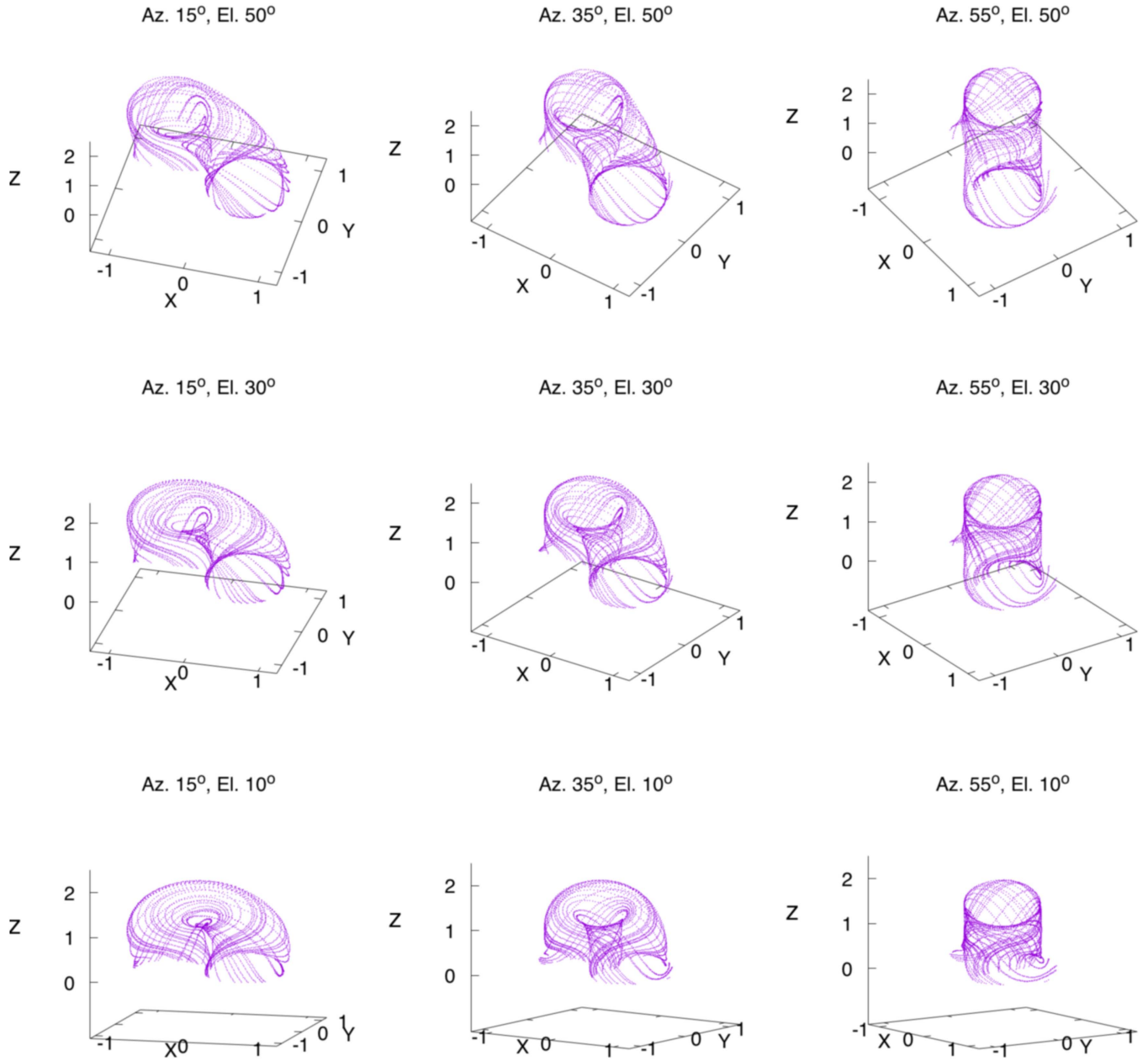

Figure 12. The mathematical representation of our 3D geometrical model, with the Cartesian axes included, and viewed from different angles. This was constructed using the theory described in the Appendix.

writhed centerline of the rope:

$$\boldsymbol{r}_{\rm twist}(t) = r_t \boldsymbol{M}_{\rm loop} \boldsymbol{M}_w \begin{pmatrix} 0 \\ \cos(t\omega_t + \phi_t) \\ \sin(t\omega_t + \phi_t) \end{pmatrix}.$$

Summing the three offset terms yields the geometry of a single twisted, writhed field line curve:

$$\boldsymbol{r}_{\rm field} = \boldsymbol{r}_{\rm loop}(t) + \boldsymbol{r}_w(t) + \boldsymbol{r}_{\rm twist}(t). \quad (1)$$

Note that Equation (1) does not necessarily define a solution to the MHD or reduced MHD system in question—it merely describes the simplest possible curve with parametrically set writhe and twist about a semicircular centerline. It does, however, capture the generic geometric behavior of such curves.

To produce our geometric CME model, we arbitrarily set $\phi_w = \pi/2$, $\omega_w = 2$, and $r_w = 0.5$ to produce a generically writhed centerline with about 30° of offset between the loop footpoints and the angle at the top of the loop. The twist direction and writhe direction have the same sense in writhed flux ropes (e.g., Canfield et al. 1999), and so we chose $\omega_t = 2$ and $r_t = 0.5 \pm \Delta r_t$, where Δr_t is a sample of a Gaussian random variable with variance 0.1 and mean 0, and ϕ_t sampled from a uniform random variable covering 0–2π. Each such sample produced a field line with reasonable twist and writhe parameters and a twist radius close to half the loop major

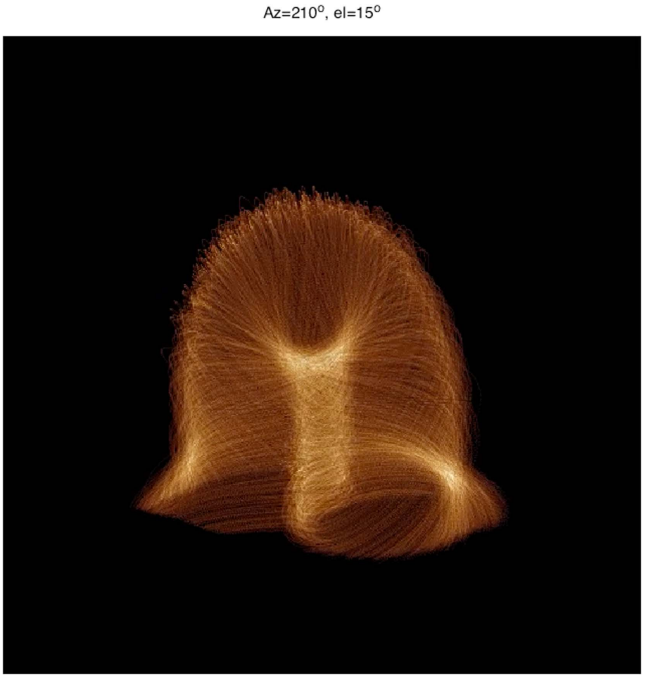

Figure 13. Animation of our 3D model showing the simplified basic geometry of a twisted, kinked flux rope (produced using the theory in the Appendix). The viewing angle is held at a fixed elevation (el = 15°) geometry and rotated about a single axis (Az) over a full 360°. We found that by observing the model from particular angles, we can reproduce the coronagraph images of CMEs quite well (Figures 10 and 11), even in this oversimplified case.

(An animation of this figure is available.)

radius. We selected 1500 such field lines, and rendered 720 points from each one onto an image plane using a simple projection matrix. Figure 12 shows the geometrical model in its mathematical context, with Cartesian axes shown. We have provided a series of images from a range of incrementally-changing projection angles in the accompanying online animated Figure 13.

REFERENCES

Anzer, U., & Tandberg-Hanssen, E. 1970, SoPh, 11, 61
Athay, R. G. 1968, in Resonance Lines in Astrophysics (Boulder, CO: NCAR), 241
Athay, R. G. 1970, SoPh, 12, 175
Athay, R. G., & Illing, R. M. E. 1986, JGR, 91, 10961
Athay, R. G., Low, B. C., & Rompolt, B. 1987, SoPh, 110, 359
Athay, R. G., & Moreton, G. E. 1961, ApJ, 133, 935
Bothmer, V., & Schwenn, R. 1994, SSRv, 70, 215
Bothmer, V., & Schwenn, R. 1998, AnGeo, 16, 1
Breit, G. 1925, JOSA, 11, 465
Brueckner, G. E., Howard, R. A., Koomen, M. J., et al. 1995, SoPh, 162, 357
Burlaga, L. F., Klein, L. W., Sheeley, N. R., Jr., et al. 1982, GeoRL, 9, 1317
Cane, H. V., Kahler, S. W., & Sheeley, N. R., Jr. 1986, JGR, 91, 13321
Canfield, R. C., Hudson, H. S., & McKenzie, D. E. 1999, GeoRL, 26, 627
Carlyle, J., Williams, D., van Driel-Gesztelyi, L., et al. 2014, ApJ, 782, 87
Chen, J. 1996, JGR, 101, 27499
Eyles, C. J., Harrison, R. A., Davis, C. J., et al. 2009, SoPh, 254, 387
Fan, Y., & Gibson, S. E. 2003, ApJL, 589, L105
Fan, Y., & Gibson, S. E. 2004, ApJ, 609, 1123
Fong, B., Low, B. C., & Fan, Y. 2002, ApJ, 571, 987
Forbes, T. G. 2000, JGR, 105, 23153
Gilbert, H. R., Alexander, D., & Liu, R. 2007, SoPh, 245, 287
Gilbert, H. R., Hansteen, V. H., & Holzer, T. E. 2002, ApJ, 577, 464
Gilbert, H. R., Inglis, A. R., Mays, M. L., et al. 2013, ApJL, 776, L12
Gosling, J. T., Hildner, E., MacQueen, R. M., et al. 1976, SoPh, 48, 389
Heinzel, P., Bommier, V., & Vial, J. C. 1996, SoPh, 164, 211
Howard, R. A., Moses, J. D., Vourlidas, A., et al. 2008, SSRv, 136, 67
Howard, T. A. 2015a, ApJ, 806, 175
Howard, T. A. 2015b, ApJ, 806, 176
Howard, T. A. 2015c, JSWSC, 5, A22
Howard, T. A., & DeForest, C. E. 2012, ApJ, 752, 130
Howard, T. A., & DeForest, C. E. 2014, ApJ, 796, 33
Howard, T. A., & Pizzo, V. J. 2016, ApJ, 824, 92
Hyder, C. L. 1965, ApJ, 141, 1382
Illing, R. M. E., & Athay, R. G. 1986, SoPh, 105, 173
Illing, R. M. E., Landman, D. A., & Mickey, D. L. 1975, SoPh, 45, 339
Illing, R. M. R., & Hundhausen, A. J. 1985, JGR, 90, 275
Innes, D. E., Cameron, R. H., Fletcher, L., Inhester, B., & Solanki, S. K. 2012, A&A, 540, L10
Joselyn, J. A., & McIntosh, P. S. 1981, JGR, 86, 4555
Kilper, G., Gilbert, H., & Alexander, D. 2009, ApJ, 704, 522
Landman, D. A., & Illing, R. M. E. 1976, A&A, 49, 277
Landman, D. A., Illing, R. M. E., & Mongillo, M. 1978, ApJ, 220, 666
Lemen, J. R., Title, A. M., Akin, D. J., et al. 2012, SoPh, 275, 17
Lepri, S. T., & Zurbuchen, T. H. 2010, ApJL, 723, L22
Lin, J., Raymond, J. C., & van Baollegooijen, A. A. 2004, ApJ, 602, 422
Linker, J. A., Lionello, R., & Mikić, Z. 2001, JGR, 106, 25165
Low, B. C. 1993, BAAS, 25, 1218
Lynch, B. J., Antiochos, S. K., MacNeice, P. J., Zurbuchen, T. H., & Fisk, L. A. 2004, ApJ, 617, 589
Martin, S. F., Livi, S. H. B., & Wang, J. 1985, AuJPh, 38, 929
Mierla, M., Chifu, I., Inhester, B., Rodriguez, L., & Zhukov, A. 2011, A&A, 530, L1
Minnaert, M. 1930, ZA, 1, 209
Munro, R. H., Gosling, J. T., Hildner, E., et al. 1979, SoPh, 61, 201
Poland, A. I., & Munro, R. H. 1976, ApJ, 209, 927
Rachmeler, L. A., DeForest, C. E., & Kankelborg, C. C. 2009, ApJ, 693, 1431
Reeves, K. K., Linker, J. A., Mikić, Z., & Forbes, T. G. 2010, ApJ, 721, 1547
Rudawy, P., & Heinzel, P. 1992, SoPh, 138, 123
Schmahl, E., & Hildner, E. 1977, SoPh, 55, 474
Schwenn, R., Rosenbauer, H., & Muehlhaeuser, K.-H. 1980, GeoRL, 7, 201
Sharma, R., & Srivastava, N. 2012, JSWSC, 2, A10
Skoug, R. M., Bame, S. J., Feldman, W. C., et al. 1999, GeoRL, 26, 161
Sturrock, P. A. 1989, SoPh, 121, 387
Sun, J. Q., Cheng, X., Ding, M. D., et al. 2015, NatCo, 6, 7598
Thompson, B. J., & Young, C. A. 2016, ApJ, 825, 27
Thompson, W. T., Wei, K., Burkepile, J. T., Davilla, J. M., St., & Cyr, O. C. 2010, SoPh, 262, 213
Török, T., & Kliem, B. 2003, A&A, 406, 1043
Török, T., & Kliem, B. 2005, ApJL, 630, L97
Tousey, R. 1973, in Space Research XIII, ed. M. J. Rycroft & S. K. Runcorn (Berlin: Akademie-Verlag), 713
Tripathi, D., Bothmer, V., & Cremades, H. 2004, A&A, 422, 337
van Ballegooijen, A. A., & Martens, P. C. H. 1989, ApJ, 343, 971
Vial, J.-C., & Engvold, O. (ed.) 2015, Solar Prominences, Astrophysics and Space Science Library, Vol. 415 (New York: Springer)
Vranjes, J., Tanaka, M. Y., Kono, M., & Poedts, S. 2004, PhPl, 11, 4188
Webb, D. F., & Hundhausen, A. J. 1987, SoPh, 108, 383
Wood, B. E., Howard, R. A., & Linton, M. G. 2016, ApJ, 816, 67
Yao, S., Marsch, E., Tu, C.-Y., & Schwenn, R. 2010, JGR, 115, A05103
Yashiro, S., Gopalswamy, N., Michalek, G., et al. 2004, JGR, 109, A07105
Zhang, M., & Low, B. C. 2004, ApJ, 600, 1043
Zuccarello, F. P., Bemporad, A., Jacobs, C., et al. 2012, ApJ, 744, 66